Coincident In Situ and W-Band Radar Measurements of Drop Size Distribution in a Marine Stratus Cloud and Drizzle

J. GALLOWAY, A. PAZMANY, J. MEAD, AND R. E. MCINTOSH

Microwave Remote Sensing Laboratory, University of Massachussetts—Amherst, Amherst, Massachussets

D. LEON, J. FRENCH, S. HAIMOV, R. KELLY, AND G. VALI

Department of Atmospheric Science, University of Wyoming, Laramie, Wyoming

(Manuscript received 25 November 1997, in final form 15 June 1998)

ABSTRACT

Investigation of precipitation formation requires measurements of the drop size distribution in a cloud. These measurements have usually been made using ground-based radar systems or aircraft in situ probes. Difficulties encountered in practice using these systems include accounting for the air motion at points remote from the radar systems and small sample volumes measured using the aircraft probes. An airborne W-band radar system provides a measurement from a much larger sample volume, close to the aircraft, with a correction for air motion possible using the data from the aircraft inertial navigation system. The Coastal Stratus Experiment conducted off the coast of Oregon in late 1995 provided W-band radar and microphysical probe data sampled from much of the same region of a marine stratus cloud. The unique combination of cloud probes and W-band radar on board the University of Wyoming King Air allowed the radar sampling to be only 60 m away from the probe sampling region. Doppler spectrum data from the W-band radar were used to produce estimates of the drop size spectrum density $N(D)$. These estimates were compared to measurements of $N(D)$ taken by the Particle Measuring Systems forward scattering spectrometer, 1D, and 2DC probes. This comparison suggests that a vertically pointing airborne W-band radar is a viable remote sensing tool for measuring $N(D)$ in clouds and precipitation. This radar provides information on drop size distribution variation on a much smaller horizontal scale than the probes as a result of the much higher sample rate and larger measurement sample volume.

1. Introduction

During September of 1995, measurements of coastal stratus clouds were made in Oregon using the University of Wyoming King Air and an airborne W-band radar. The purpose of the measurements was to study precipitation initiation. The radar used was the new Wyoming Cloud Radar (WCR) installed in June 1995 on the University of Wyoming King Air. This radar is a fully polarimetric, coherent W-band system with pulse-to-pulse programmable transmit polarization and horizontally (H) and vertically (V) polarized receiver channels. The Doppler spectrum of the return signal from the coastal stratus cloud was measured at vertical incidence using H polarization only. This measurement provides an opportunity to examine the degree of correlation between the estimates of the drop size distribution made by the radar and the observations available from the wingtip probes on the King Air. For the data analyzed in this study, the probes provide a measurement of the drop size spectrum at the flight level, and the radar provides data from a much larger volume about 60 m above the aircraft.

Doppler spectrum measurements of liquid water clouds and precipitation provide much of the necessary information to determine the drop size density spectrum $N(D)$; the reflectivity $Z_{e\mathrm{HH}}$; and the mean, reflectivity weighted velocity toward the radar, $\overline{v}_D$. Reflectivity and velocity are simply moments of the measured Doppler spectrum, while estimation of $N(D)$ requires a known relation between the fall velocity of the drops and their diameters. A comprehensive review of the efforts to use Doppler radar systems to characterize the drop size distribution in rain appears in Atlas et al. (1973). This review indicated that prior efforts to use ground-based radars to make measurements of the drop size distribution had been hampered by the difficulty of establishing the local vertical air motion, which has a strong effect on the computed drop size distribution. More recently, efforts to make use of wind profilers for similar measurements have met with success (see Gossard 1988 and Rogers et al. 1993). Measurement of the drop size

Corresponding author address: Dr. John C. Galloway, Microwave Remote Sensing Lab, University of Massachusetts, 211C Knowles Engineering Bldg., Amherst, MA 01003.
E-mail: galloway@mirsl.ecs.umass.edu

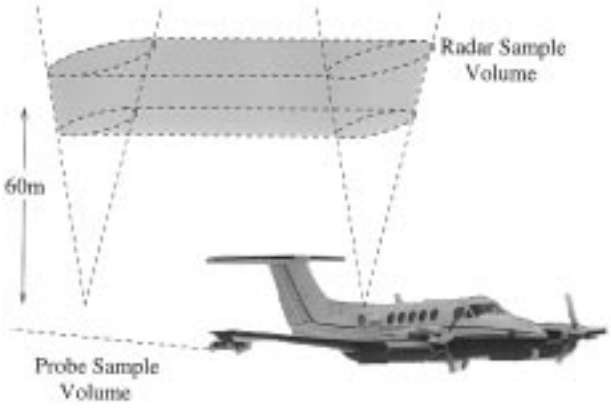

FIG. 1. Diagram of King Air sweeping out sample volumes for radar and microphysical probe measurements.

distribution in heavy rain is possible with a W-band system as a result of the updraft-induced shift in the onset of Mie region backscatter effects in the measured spectrum (Lhermitte 1988). The King Air platform is unique in that measurements of vertical air motion by the aircraft inertial navigation system can be used to correct the velocity measured by the W-band radar. Using this velocity data allows estimates of the drop size distribution to be produced without making assumptions about the shape of the drop size spectrum. Furthermore, the drop size distribution is not required to have drops large enough to produce Mie region backscatter.

The following sections discuss the measurements and their interpretation. The first section presents a description of the radar and particle probes. A discussion of the method used to make Doppler spectrum measurements with the W-band radar follows. The third section describes details of the calculation of drop size distributions using the Doppler spectrum data and microphysical probe data. This is followed by sections discussing the expected accuracy and precision of the $N(D)$ estimates from the radar and probes. A brief description of the environmental conditions prevailing during the measurement is followed by a section covering the results of the analysis. This section starts with direct comparisons of the $N(D)$ estimates from the radar and the probes for a selected point in the available data. A more detailed analysis of the concentration density estimates compared between the two systems for a number of diameter bins completes the direct comparison of the $N(D)$ estimates. Comparison of the spectral properties along track for both the 2DC (Baumgardner 1989) and radar measurements follows. The paper concludes with a discussion of what has been established with this particular set of measurements.

2. Instruments

a. W-band radar

The University of Wyoming 95-GHz airborne cloud radar is a pulsed, fully coherent, dual-receiver polarimetric radar system with programmably switched linear (H and V) polarization from pulse to pulse. An antenna mounted to the fuselage of the King Air is shielded by a faring containing a motor-driven reflector plate and two dielectric windows, providing the capability to direct the radar beam up or to the side during flight (see Fig. 1). The outputs of the two receivers are sampled by digitizers that stream data to Digital Signal Processors (DSPs) running in parallel for data preprocessing. A system control computer configures and runs the DSPs and an arbitrary function generator that is used to control the transmitter and polarization switching network. The entire data acquisition system is contained in a VXI mainframe that provides the power supply and necessary cooling. System specifications may be found in Table 1. Further information on this radar may be found in Pazmany et al. (1994), which discusses the details of a similar polarimetric radar system developed for the King Air by the University of Massachusetts—Amherst.

TABLE 1. 95-GHz radar specifications for King Air facility.

Transmit frequency	94.92 GHz
Peak power	1.2 kW
Pulse duration	100 ns (15 m) or 200 ns (30 m)
Pulse repetition frequency	15 kHz
Antenna diameter	30.5 cm
Antenna beam width	0.7°
Receiver noise figure	11 dB (SSB)
Receiver bandwidth	5 MHz
Minimum detectable reflectivity	-22 dBZ_e (1-km range, 200-ns pulse)

b. Probes

The probes available on the King Air include the Particle Measuring Systems forward scattering spectrometer (FSSP), 1D, and 2DC probes (see Fig. 1 for the position of the probes on the wing). The drop size distribution is measured directly at flight level with each of these probes over a size range specific to each probe. The regions of overlap between probes are usually resolved by taking the probe focused on the smaller diameter regime to be the more correct instrument for a given diameter in an overlap region. This was done to avoid biases induced by a lack of sensitivity to small drops on the part of the probes focused on the larger drop diameters. Estimates of the moments of the drop size distribution, such as reflectivity and liquid water content, are calculated directly from the measured spectra for a given probe. Discussion of the measurement technique applied for each probe and its limitations and accuracy may be found in Baumgardner (1983), Heymsfeld and Parrish (1978), and Cerni (1983).

3. Doppler spectrum measurement technique

During the Coastal Stratus Experiment, the radar sampled groups of 64 pulses, all H polarization, at 15 kHz

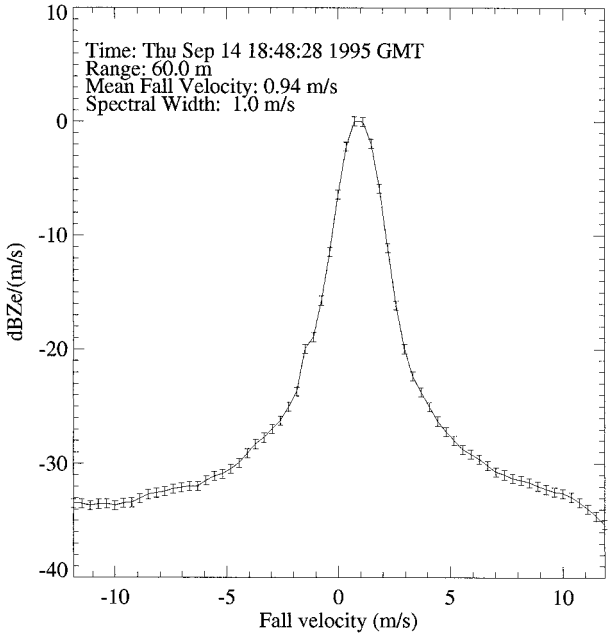

FIG. 2. Example Doppler spectrum measurement from 14 September 1995 during Coastal Stratus Experiment, 1-s averaging interval. Error bars on plot indicate expected range ($\pm\sigma$) for single standard deviation of power measurements.

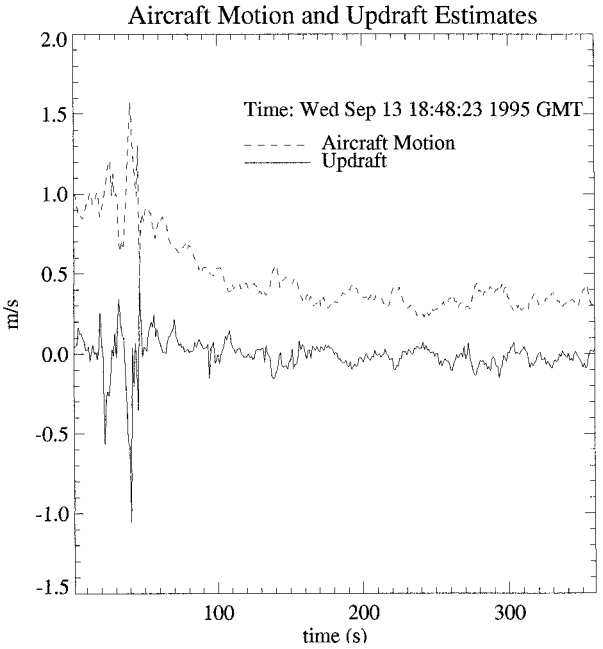

FIG. 3. Aircraft motion and wind component along radar beam (called the updraft in this case in analogy with a ground-based system looking up) for 14 September case.

(sample period, $T_s = 66.7\ \mu$s) to form the Doppler spectrum estimates. A real-time DSP-based signal processing system calculated a periodogram from each group of 64 samples. Eight such estimates were formed and averaged for each of the Doppler spectrum estimates that were recorded at a rate of 15.5 Hz. This processing was done for each of the 100 range gates separated by 15 m (100 ns), starting at a range of 60 m. This places the first gate at the beginning of the far field of the antenna. An example of a processed, postaveraged (1-s along track) Doppler spectrum corrected for aircraft motion appears in Fig. 2. Plots of the aircraft velocity and wind velocity components into the radar beam are provided in Fig. 3. These velocity measurements provide the correction necessary to translate the measured Doppler velocity to fall velocity.

4. Estimation of drop size distribution from Doppler spectra

After removing the velocity offset due to aircraft motion, subsequent averaging of the Doppler spectrum estimates along track was performed to match the intervals at which 2DC and 2DP data were reported (1 s or about 85 m along track for this case). The resultant number of periodograms averaged for each averaged Doppler spectrum was 124. Since the pulse repetition frequency of the radar was 15 kHz, the folding velocity for the spectral estimates was 11.9 m s^{-1}.

The procedure used for inverting the Doppler spectra to drop size distributions assumes that the measured spectra are related to the drop distribution by the following [Doviak and Zrnić 1993, their Eq. (8.77)]:

$$S_n(w - w_t)dw_t = \frac{\sigma_b(D)N(D)dD}{\eta}, \tag{1}$$

where $S_n\,(w - w_t)$ is the measured spectrum normalized to the total reflectivity, $\eta\ [=\int_0^\infty \sigma_b(D)N(D)\,dD]$, shifted by the amount required to remove vertical air motion (w); w_t is the terminal fall speed of the drops of a given diameter D; σ_b is the volume backscatter coefficient; and $N(D)$ is the drop size distribution in terms of drop diameter.

Inversion of $S_n(w - w_t)$ to $N(D)$ is accomplished by solving (1) for $N(D)$:

$$\frac{S_n(w - w_t)\eta}{\sigma_b(D)}\frac{dw_t}{dD} = N(D), \tag{2}$$

where the values for $\sigma_b(D)$ may be calculated for spherical drops of water using Mie's solution for backscatter from dielectric spheres (Mie 1908). For the purposes of this analysis, the form of the Mie solution developed by Deirmendjian and presented in Ulaby et al. (1982a) was used.

The velocity for a particular bin, v_k, including the effect of aircraft motion, is

$$v_k = k\frac{\lambda}{2MT_s} + v_{\text{acbeam}} + v_{\text{updraft}} \qquad -\frac{M}{2} \le k \le \frac{M-1}{2}, \tag{3}$$

where λ is 3.16 mm, T_s is the pulse repetition period

(PRT) (66.7 or 200 μs), v_{acbeam} is the component of aircraft motion lying along the radar beam, v_{updraft} is the wind component along the radar beam, and M is the number of FFT bins.

The relation between w_t and D used to find the drop diameters corresponding to the measured velocities was one proposed in Rogers et al. (1993):

$$w_t(D) = \begin{cases} KD(1 - e^{-kD}), & D \le D_0, \\ A - Be^{-CD}, & D \ge D_0, \end{cases} \quad (4)$$

where $K = 4$ m s^{-1} mm^{-1}, $k = 12$ mm^{-1}, $A = 9.65$ m s^{-1}, $B = 10.43$ m s^{-1}, $C = 0.6$ mm^{-1}, and $D_0 = 0.745$ mm. This relation was principally chosen due to its tractable nature in carrying out the derivative required in (2). A correction for air density was also applied using the pressure and temperature measurements available from the King Air sensors. The relationship used for correction from air at a reference density of ρ_0 given a temperature, T_0, of 293 K, and reference pressure, P_0, of 760 mm Hg was (Doviak and Zrnić 1993, section 8.2):

$$w_t(D, \rho) = w_t(D)\left(\frac{T_0 P}{T P_0}\right)^{0.5}, \quad (5)$$

where ρ is the air density at a temperature of T and pressure of P. The choice of 0.5 as the exponent for use when drop fall velocities are small (<2.5 m s^{-1}) was guided by the discussion on the topic in Gossard (1994).

Given the calibrated values of reflectivity available from the radar spectra measured along track in the closest range gate, and the spectra normalized to these reflectivities, the procedure used to calculate the radar estimates of $N(D)$ was as follows.

1) Shift each measured spectrum in velocity by an amount equal to $v_{\text{acbeam}} + v_{\text{updraft}}$ so that the resulting spectrum is plotted relative to drop fall velocity.
2) Average as many Doppler spectra as needed to match the averaging time of the particle probes.
3) Find the values of w_k, the estimated fall velocity, that remain greater than zero. (Find all k such that: 8.1 m s^{-1} > w_k > 0 m s^{-1}.)
4) Calculate the drop diameters, D_k, and derivatives of drop velocity, dw_t/dD, corresponding to w_k for all usable k.
5) Use (2) to calculate the values of $N(D_k)$ for all available k.

Note that the units used for the quantities were m^2 m^{-3} for η, meters for all lengths, and seconds for time. This led to units of m^{-3} m^{-1} for calculated values of $N(D_k)$.

5. Drop size distribution available from probe data

The data available from the aircraft probes includes that from the FSSP, 1D, and 2DC probes (Baumgardner 1989). Values of the drop size distribution are reported for the FSSP probe in units of cm^{-3} μm^{-1} in 3-μm intervals from 3 to 45 μm. Those for the 1D probe are reported in units of L^{-1} at intervals of 12.5 μm from 12.5 to 187.5 μm. The values for the cumulative 2DC distribution are reported in units of L^{-1}. To plot the drop size distribution data from the probes on the same scale as the radar estimate of $N(D)$, the drop distributions from the FSSP and 1D probes, N_{FSSPm} and N_{1Dm}, must be scaled appropriately to units of m^{-3} m^{-1}. The relations for the plotted versus the reported distributions for the FSSP and 1D probes are

$$N_{\text{FSSP}}(\text{m}^{-3}\ \text{m}^{-1}) = N_{\text{FSSPm}}(\text{cm}^{-3}\ \mu\text{m}^{-1})\frac{\text{m}^{-1}}{(10^6\ \mu\text{m})^{-1}}\frac{\text{m}^{-3}}{(10^2\ \text{cm})^{-3}} \quad (6)$$

and

$$N_{\text{1D}}(\text{m}^{-3}\ \text{m}^{-1}) = N_{\text{1Dm}}(\text{L}^{-1})\frac{\text{m}^{-3}}{(10^3\ \text{L})^{-1}}\frac{1}{12.5\ \mu\text{m}}\frac{\text{m}^{-1}}{(10^6\ \mu\text{m})^{-1}}. \quad (7)$$

The 2DC distribution, F_{2DC}, must be both differentiated and scaled to arrive at comparable values. The calculation and scaling of the first derivative were performed as follows:

$$N_{\text{2DC}}[i](\text{m}^{-3}\ \text{m}^{-1}) = (F_{\text{2DC}}[i] - F_{\text{2DC}}[i+1])(\text{L}^{-1}) \times \frac{2}{(dD_{\text{2DC}}[i] + dD_{\text{2DC}}[i+1])}\frac{\text{m}^{-3}}{(10^3\ \text{L})^{-1}}, \quad 0 \le i \le N_{\text{diams}} - 2, \quad (8)$$

where $dD_{\text{2DC}}[i]$ is the bin width for the ith point of the cumulative distribution.

6. Expected errors in measurements of Doppler spectrum and $N(D)$

a. Expected sources of distortion in Doppler spectra

Many effects other than the drop size distribution itself contribute to the measured Doppler spectrum shape. Among the more significant effects were the finite antenna beamwidth and aircraft motion. The expected contributions of aircraft motion and finite beamwidth to the measured spectrum may be approximated by a Gaussian spectrum convolved with the desired spectrum to result in the measured spectrum. This distortion spectrum is centered at the velocity equal to the component of forward motion of the aircraft into the radar beam. The width of the spectrum used to describe this distortion is (see Doviak and Zrnić 1993, section 5.2)

$$\sigma^2 = 0.09 v_a^2 \theta_1^2. \quad (9)$$

In this case, θ_1 is the one-way, half-power beamwidth

of the radar antenna; and v_a is the component of aircraft motion bringing about the increase in spectrum width. This component was taken to be the airspeed since the radar look direction and aircraft motion vector were nearly perpendicular.

Another component of the distortion expected in the measured Doppler spectra is the windowing effect on the measured spectrum. No window was used on the time series of returns processed in the DSP subsystem, so the spectral window associated with a rectangular window in the time domain applies in this case. The resultant spectrum is the circular convolution of this spectral window with the desired spectrum (Oppenheim and Schafer 1989). This spectral window has the form

$$W(v) = \sin^2(\pi L v/2v_N) \sin^{-2}(\pi v/2v_N), \quad (10)$$

where v is the Doppler velocity, v_N is the folding velocity $[\lambda(4T_s)^{-1}]$, and L is the number of samples used to form the spectrum (64 in this case). It should be noted at this point that although some attempts have been made at deconvolving the two forms of distortion mentioned here from the available measurements, no results presented in this paper have had these components successfully removed from the measured Doppler spectra. That removal will have to wait for future efforts.

b. Precision expected in N(D) estimates from Doppler spectra

The precision in the measurement of power at each bin of the Doppler spectrum determines the precision with which the estimates of $N(D)$ are formed for the radar estimate of the drop size spectrum. The power estimates for each point in a periodogram of a Rayleigh fading signal are distributed exponentially (see Jenkins and Watts 1968, section 6.3.1 for a discussion of why). This means that the variance of each of the power measurements equals the square of the mean value (Doviak and Zrnić 1993). Details of calculating the standard deviation of the power measurement for a given bin after noise subtraction appear in Ulaby et al. (1982b). The result in terms of the mean power measurement at each bin of the periodogram is

$$\frac{\sigma_P}{\overline{P}} = \frac{1}{M^{1/2}}\left(1 + \frac{1}{\text{SNR}}\right)^{1/2} + \frac{1}{M_n^{1/2}}\left(\frac{1}{\text{SNR}}\right)^{1/2}, \quad (11)$$

where M is the number of periodograms averaged, M_n is the number of noise samples, SNR is the single pulse signal-to-noise ratio, $\overline{P}$ is the sample mean of the measured power, and σ_P is the expected standard deviation of the power measurement.

The SNR at the nearest range gate was well above 20 dB for all points in the spectrum, providing negligible variation in the fluctuation in the power measurement after noise subtraction. Thus, the only variation in the precision in the radar estimate of $N(D)$ was due to the number of periodograms involved in the estimate. The absolute calibration of the radar system was established using corner reflector measurements made at the airport before and after flights. A relative error in the calibration constant of 1 dB will bring about a 1-dB error in the $N(D)$ estimates from the Doppler spectra. An additional benefit from a comparison of the probe and radar measurements of the drop size distribution is verification of the calibration constant used to process the radar data.

c. Precision expected in probe measurements of N(D)

The precision of the $N(D)$ measurements from the wingtip probes depends on the number of drops, N_{drops}, counted in a particular diameter bin over an averaging interval. The counts are distributed according to a Poisson density function. Like the power measurement modeled by the exponential density, the mean count standard deviation is equal to the count. Therefore, given a density, λ, of drop observations falling into a diameter bin over an interval, Δt, the distribution of the density measurement from a probe is approximately normal with mean $\lambda\Delta t$ and standard deviation $\lambda\Delta t/\sqrt{N_{\text{drops}}}$. This distribution simply models the behavior of a perfect counting device. If the observation of concentration density for a particular diameter, D, is represented by $\hat{N}(D)$, then the expression for this value within a 95% confidence interval is

$$\hat{N}(D)\left(1 \pm \frac{1.96}{\sqrt{N_{\text{drops}}}}\right), \quad (12)$$

where N_{drops} was calculated as the product of the observed concentration density, the sample volume, and the width of the diameter bin.

The number of seconds required to achieve a measurement deviation that is 20% of the mean value with 95% confidence was calculated for a number of concentration densities and sample volumes for the 2DC probe (see Table 2). Similar results for the 1D and FSSP probes are not presented here because the 1D probe sample volume was too small to provide accurate results in the measurement time available, and the diameter range of the FSSP falls below that resolveable with the present radar data. The results for the 2DC indicate that a few seconds to a few tens of seconds are required for convergence to a given value of $N(D)$, depending on the concentration present. The probes also possess a number of device characteristics that impact the eventual accuracy and precision of the concentration measurements. Examples of these characteristics include partial obscuration of the aperture by drops, drop fragmentation on the probe housing, and calibration errors (Baumgardner 1989).

d. Comparison of sample volumes and sensitivity

The two sets of measurements, radar and probes, provide drop size density spectra averaged spatially over

TABLE 2. Values of averaging interval (in s) required to achieve a 95% confidence deviation of 20% relative to the mean for different sample volume rates and concentration density estimates. A 50-μm width bin was assumed and the 2DC probe bin widths are indicated below the corresponding sample volume rates (85 m s^{-1} airspeed assumed).

Sample volume rate Concentration density (m^{-4})	4.8 L s^{-1} 125 μm	5.1 L s^{-1} 175 μm	5.3 L s^{-1} 225 μm	5.6 L s^{-1} 275 μm	6.0 L s^{-1} 350 μm
10^6	399.95 s	379.44 s	360.94 s	344.15 s	321.70 s
10^7	40.00 s	37.94 s	36.09 s	34.41 s	32.17 s
10^8	4.00 s	3.79 s	3.61 s	3.44 s	3.22 s
10^9	0.40 s	0.38 s	0.36 s	0.34 s	0.32 s

different regions of space. The probe measurements arise from the flow of drops through the probe's field of view over a given interval. During that time, the equivalent volume sampled by the probes is determined by the sample area of the probe and the airspeed (see Baumgardner 1989 for examples of how to calculate these sample volumes). The radar sample volume is determined by the sampling density in time, the range resolution cell size, and the airspeed and is in excess of 10^5 L over a 1-s interval. The 1D probe sample volume varies over the diameter range of the device but does not exceed 1 L for a 1-s interval. The 2DC probe samples a volume of 4–40 L in a second, depending on drop diameter. The airspeed for which these sample volumes were obtained was about 85 m^{-1}.

A plot of the minimum concentration at a particular diameter for each of the three systems is provided in Fig. 4. This minimum concentration for the probes was calculated as that concentration density for a given diameter at which only a single drop was counted by the probe during the averaging interval. It should be noted that at this number of drops, the relative error of the $N(D)$ observation is 100%. The minimum concentration for the radar was determined from the system thermal noise threshold level mapped to the equivalent value of $N(D)$. The first null in backscatter efficiency due to Mie resonance shows up in Fig. 4 as a sharp increase in retrieved $N(D)$ at around 2×10^{-3} m diameter. This aspect of the retrieval process is not relevant in the current context since the drop densities for large diameter drops are below the threshold for both the probes and the radar. However, attempts to retrieve $N(D)$ in heavier precipitation situations would need to address this feature.

The radar and 2DC probe have similar sensitivity for drops around 100–200 μm but diverge substantially in sensitivity for smaller and larger drops. For this case, the drop concentrations in diameter bins smaller than 100 μm fell above the radar's minimum sensible concentration. The observed concentration densities from the 2DC system are not reliable below 100 μm since the pixel resolution for the 2DC images is 25 μm. Values from the 1D and FSSP probes are preferred in these diameter ranges.

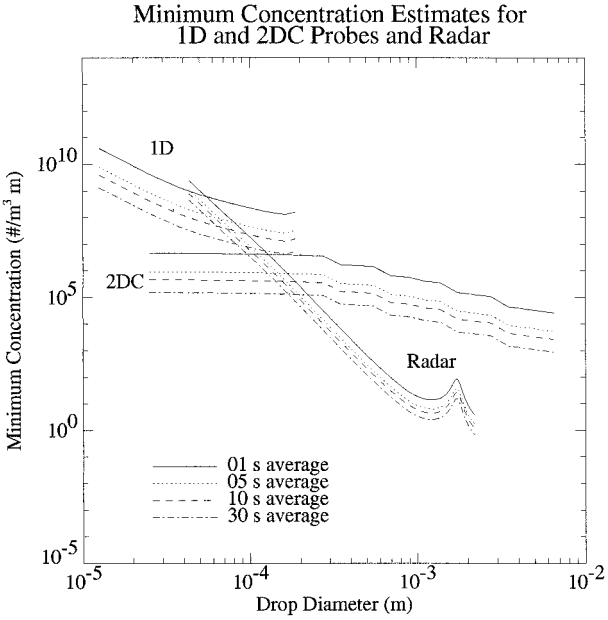

FIG. 4. Comparison of sensitivities of radar, 1D, and 2DC probes in terms of minimum $N(D)$ measurement possible for different averaging intervals.

e. Impact of velocity offsets on radar N(D) estimate

Error in estimation of the fall velocity associated with a given spectral estimate impacts the eventual $N(D)$ estimate in two ways. Both the backscatter cross-section calculated for a given diameter associated with a fall velocity and the derivative of velocity with diameter depend strongly on the absolute value of the fall velocity. In particular, the cross-section values vary as the sixth power of the estimated particle size in the Rayleigh backscatter region, so that error propagated through the transformation from velocity to diameter provides a principal source of the error in the estimates of $N(D)$. Figure 5 displays the impact of this error on $N(D)$ estimates for a variety of simple shifts of the velocity axis, which could result from errors in the aircraft motion measurement or the estimate of the updraft velocity.

The theoretical value of $N(D)$, plotted in Fig. 5 as the 0 m s^{-1} case, was taken to be that from a Marshall–Palmer distribution ($N_0 = 5.6 \times 10^9$ m^{-4}, $\Lambda = 13.24 \times 10^3$ m^{-1}), and a corresponding fall velocity spectrum was calculated using (1). The values of velocity were calculated from the diameters using (4). After the fall velocity spectrum was calculated, the error in velocity

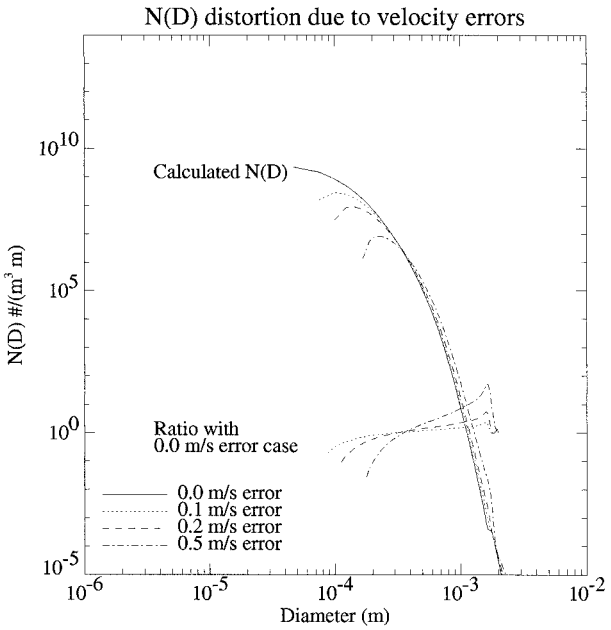

FIG. 5. Distortion in $N(D)$ estimate expected for velocity offsets vs drop diameter.

was simulated by simply adding an offset to the fall velocity axis and calculating the $N(D)$ values associated with the given spectral power estimates at the new velocities. The results of this simulation make it clear that even a small error in velocity, of around 0.5 m s^{-1} or so, can have a pronounced effect on the concentration estimates. It should be noted as well that the range of drop diameters available for $N(D)$ estimation from the measured Doppler spectra is determined by the minimum and maximum resolved velocities in the spectrum and this is influenced by the shift in the velocity axis brought about by error in both the aircraft motion compensation and updraft removal. Given the relative values of the aircraft motion and updraft velocity measurements (see Fig. 3), the aircraft motion removal was the more significant correction in this particular case.

The possible sources of distortion in the measured Doppler spectrum include more effects than just simple offsets in velocity. Spreading of the measured Doppler spectrum arises from turbulence, the uniform air motion across the resolution volume brought about by aircraft motion, and the windowing involved in sampling the return signal. Given the airspeed and assuming a Gaussian antenna pattern, (9) indicates that a spectrum of about 0.3 m s^{-1} width was convolved with the desired result to yield the measurement. Measurements of turbulence were made using an MRI turbulence meter, an analog device with a transducer in the King Air nose boom making a direct measurement of airspeed fluctuations (Meteorology Research, Inc. 1969), and this data could be used to estimate an upper bound on the effect turbulence had on the Doppler spectrum measurements. Finally, simulation of the expected Doppler spectrum could be used to establish the impact of sampling on the measured spectra.

7. Description of 14 September case

During one period on 14 September 1995, the King Air flew just above the surface (140 m) for about 30 km through light drizzle and a marine stratus cloud. The image of the reflectivity as integrated from the measured Doppler spectra indicates that the stratus cloud extended about 300 m above the aircraft flight level (see Fig. 6). The reflectivity and measured fall velocity for a 10-s interval along track are also displayed with the indication of the region in the larger-scale image from which data were sampled. This interval corresponds to the 10-s averaging interval considered in the next section. The measured fall velocity depicted in Fig. 6 includes the correction for aircraft motion but not the updraft estimate applied to find the actual fall velocity spectrum for use in drop size distribution estimation. The temperature at flight level was 12.3°C and the pressure was 995 mb.

The indicated turbulence along track as measured by the MRI turbulence meter was less than 0.5 $(cm^2\ s^{-3})^{1/3}$. Assuming that the dimensions of the radar resolution volume were small compared with the extent of the inertial subrange for this case, the expected impact of the turbulence on the Doppler spectra would be a convolution of a spectrum of about 0.05 m s^{-1} width, which is negligible compared with the contribution from the aircraft motion and the expected ideal spectrum width. This spectrum width was determined using a result reported in Doviak and Zrnić [their 1993, Eq. (10.70)]. Given the sampling performed in this case, a simulation using a Marshall–Palmer drop size distribution was carried out to establish the expected spectrum broadening due to windowing. Using a distribution described by

$$N(D) = 4 \times 10^8\ \mathrm{m}^{-4}\ e^{-18\times10^3\ \mathrm{m}^{-1} D}, \qquad (13)$$

an ideal Doppler spectrum calculated from this drop size distribution using (1) and a simulation procedure (Zrnić 1975) for generating time series from Doppler spectra given an ideal spectrum, the spectrum width without distortion from the finite antenna beamwidth, and turbulence was 0.57 m s^{-1}. The addition of the finite antenna beamwidth contribution increased this value to 0.64 m s^{-1} and the windowing effect increased this to about 1 m s^{-1}. This compares well with the measured results, an example of which may be found in Fig. 2.

8. Results

The values of $N(D)$ derived from the Doppler spectra and reported by the aircraft probes may be placed on the same scales and compared by eye. This provides an initial analysis of the time required to establish a reasonable comparison between the two kinds of measurement. Since the number of such measurements is quite

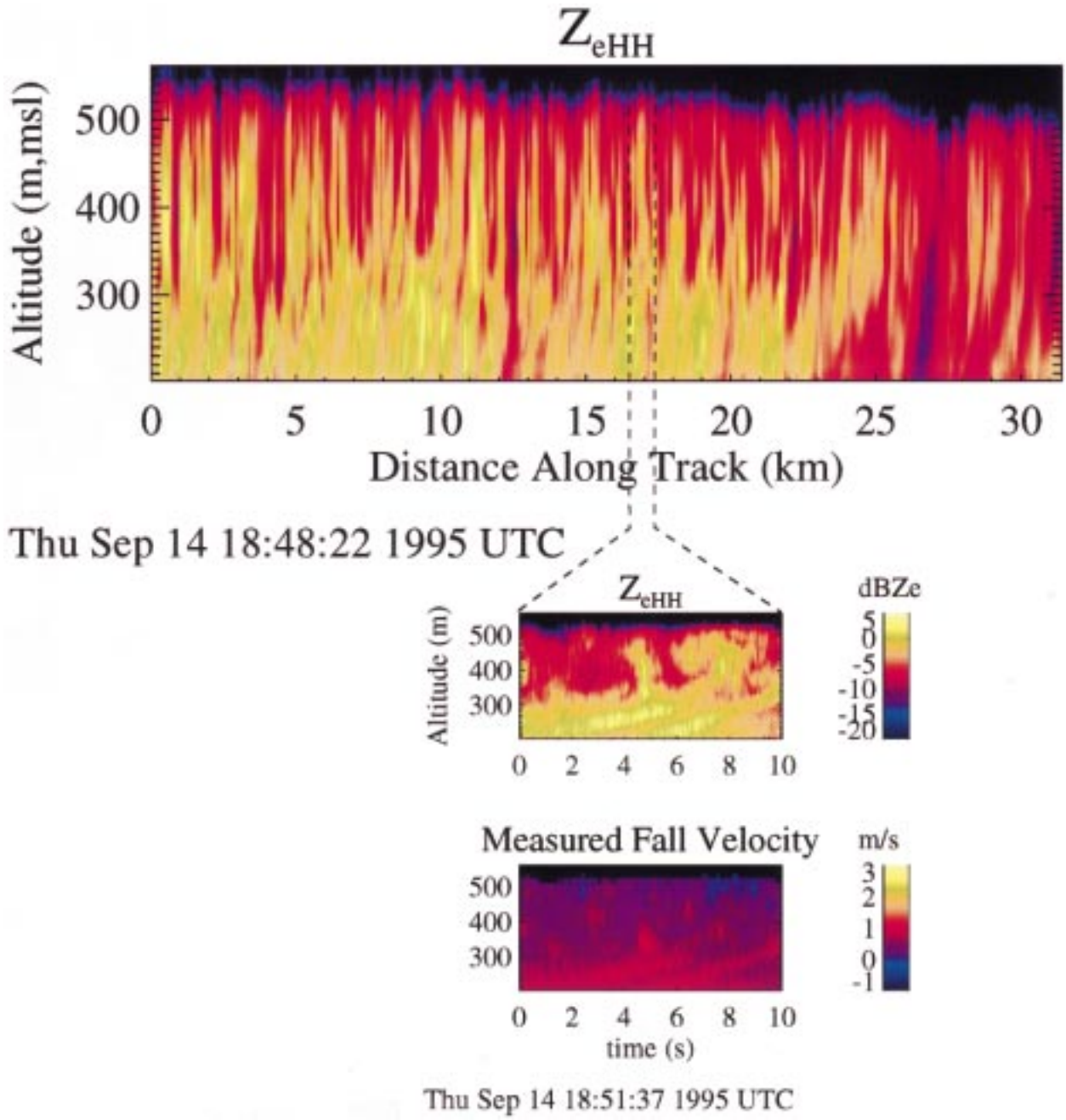

FIG 6. Large-scale and expanded-scale images of coastal stratus cloud observed on 14 September 1995.

large, however, sampling or averaging of the results must take place to provide some form of reasonable summary of the results. Given that the aircraft was flying at the lower cloud edge and passing in and out of clouds, the choice of interval over which the results are averaged will have a distinct impact on the correspondence that will be visible in the $N(D)$ estimates. Therefore, the only use of looking at individual plots of $N(D)$ is to establish the range of concentrations involved and to obtain some sense of the ranges of error present in the measurements over a particular time interval.

Since the radar sample volume falls well inside the cloud, the radar measurement has a high SNR; therefore, these measurements are not limited by instrument noise. The time windowing, however, has a substantial impact (see section 6a). The probes, on the other hand, have error driven by the mean value of the concentration, in the form of the number of drops, N_{drops}, falling into a

diameter bin over a given interval. To quantify, in a useful fashion, the degree of correlation between the two sets of measurements, two forms of time series analysis were applied. For particular diameter intervals, power spectra were calculated and compared for time series of radar concentration density estimates and probe measurements. The cross-correlation properties of the two sets of values of $N(D)$ were analyzed using integrated cospectrum and phase spectrum analysis as well.

a. Direct comparison of N(D) values

1) SELECTED PLOTS OF $N(D)$

The plots of $N(D)$ provided for comparison were taken from data centered at 200 s (17.2 km) along track in Fig. 6. This point in time corresponds to 5 s along the abscissa of the expanded scale plots in that figure. Figures 7–9 display examples of the estimated $N(D)$ values from the aircraft probes and radar data. The top panels of Figs. 7–9 are plots of $N(D)$ averaged over intervals of 1, 10, or 30 s, respectively. The 10-s average corresponds to the average taken over the first gate displayed in the expanded scale images in Fig. 6. The 30-s average corresponds to data that extends 10 s before and after the expanded scale images. The agreement between radar and probe estimates at this point along track is striking for a 1-s average. Comparison of the longer averaging interval results reveals that at this location the match between the 2DC data and the radar concentration estimates is reasonable over the 125-, 175-, and 225-μm-diameter bins. The radar threshold indicated in these plots of $N(D)$ is the minimum detectable concentration at a given diameter interval for the radar $N(D)$ estimates. This threshold was chosen to be 1 dB above the receiver thermal noise floor. The abrupt rise in concentration density with a diameter of about 2×10^{-3} m is the same as that noted in section 6d and is due to the first null in the Mie resonance region for backscatter efficiency.

The 95% confidence interval for both radar and probe measurements was calculated using the relations in (11) and (12), respectively. The lower panels in Figs. 7–9 display the ratio of the 95% confidence interval to the mean (since both measurements' standard deviations are related to their means). Values of the expected 95% confidence interval greater than 1.5 times the mean were not plotted. The 1D data settle in to a reasonable spectrum only for long averaging intervals (>10 s) and do not appear to correspond to the radar concentration density estimates except for the larger diameters covered by the 1D probe. Over the time period available, the 1D concentration density estimates did not converge beyond about 0.2 of the mean value for the 95% confidence deviation, so that further comparison of the 1D results with the radar data was not undertaken.

The expected deviation of the 2DC concentration density observations at 125, 175, and 225 μm, however,

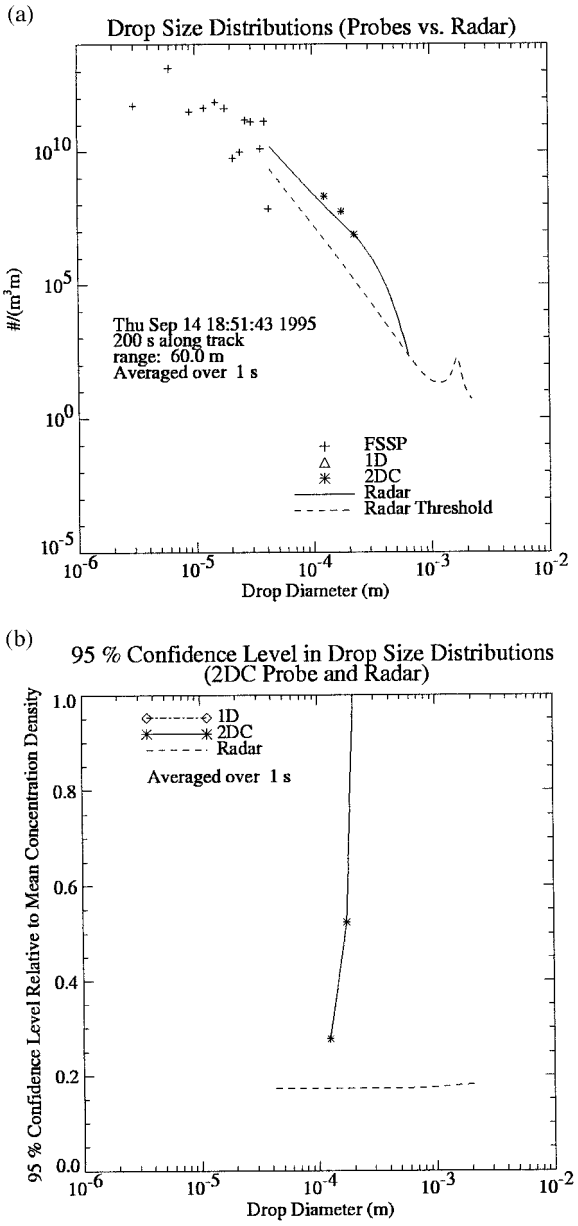

FIG. 7. The $N(D)$ estimates for both radar and probes at 200 s along track, 1-s average. The sharp rise in the radar threshold at around 2×10^{-3} m is due to the onset of Mie resonance in backscatter efficiency (see section 6d).

converged to below or around 20% of the mean value after 10 s or so, as predicted given the concentrations of drops observed (see Table 2). For this location, the velocity offset in the Doppler spectrum measurement was not large enough to bring about a substantial difference between the radar and probe results for the 125-, 175-, and 225-μm-diameter bins. Given the information from Fig. 5 and the correspondence between the $N(D)$ values from the radar and 2DC probe at 125 μm, the absolute velocity error retained in the Doppler spectrum after correction for aircraft motion should be less than

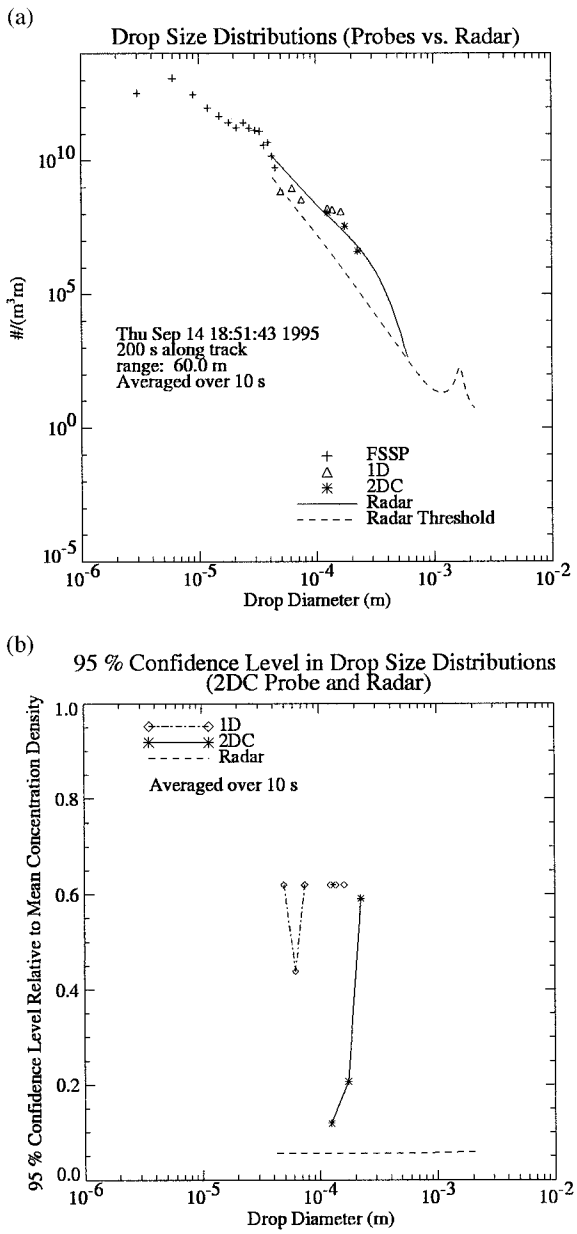

FIG. 8. The $N(D)$ estimates for both radar and probes at 200 s along track, 10-s average. The sharp rise in the radar threshold at around 2×10^{-3} m is due to the onset of Mie resonance in backscatter efficiency (see section 6d).

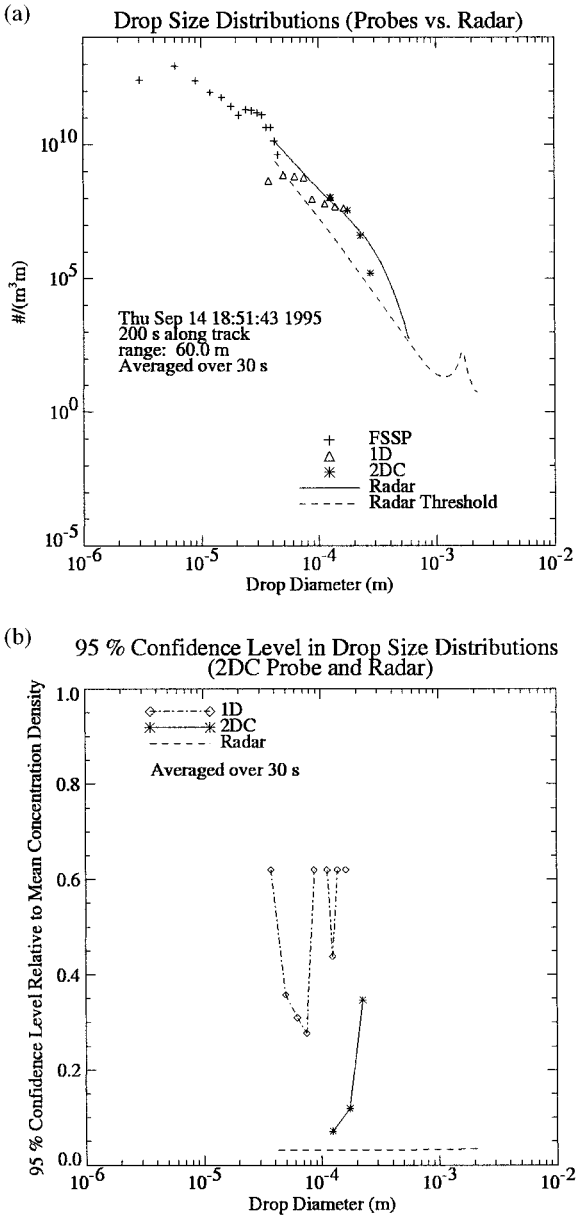

FIG. 9. The $N(D)$ estimates for both radar and probes at 200 s along track, 30-s average. The sharp rise in the radar threshold at around 2×10^{-3} m is due to the onset of Mie resonance in backscatter efficiency (see section 6d).

about 0.1 m s^{-1}. The high diameter end of the FSSP drop size spectrum (45-μm diameter) does not quite extend into the diameters covered by the radar spectrum estimate (50-μm diameter), but there is a clear correspondence between the two displayed in these plots.

2) PLOTS OF CONCENTRATIONS FOR INDIVIDUAL DIAMETERS

Scatterplots of concentration density estimates for multiple bins from the 2DC probe plotted against the corresponding radar estimates are displayed in Figs. 10–12. In these cases, the radar drop size spectrum estimates were interpolated onto the same diameter grid as the probe data. For drop diameters of 125–325 μm the radar and 2DC probe data correspond to within an order of magnitude. The values for the smallest diameter bin, 75 μm, are higher for the radar estimates than the 2DC probe measurements. This is to be expected since the pixel resolution of the 2DC probe, 25 μm, makes reliable measurements of particle concentration densities impossible for diameters below about 100 μm.

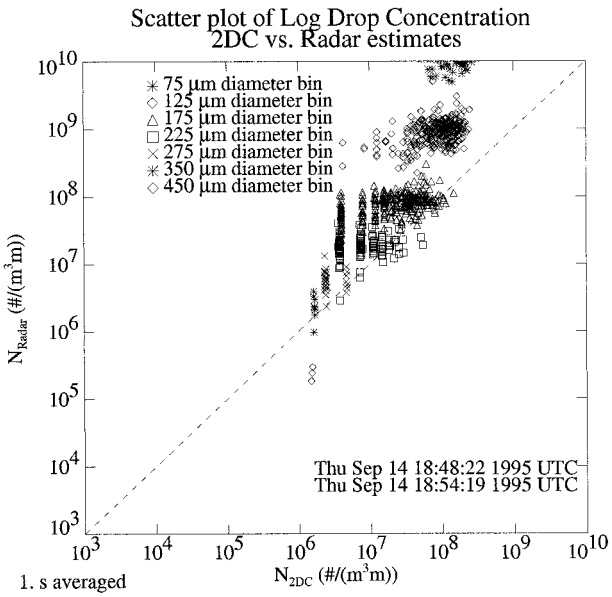

FIG. 10. Scatterplot of concentrations measured by 2DC and corresponding radar estimates of $N(D)$ for diameter bins reported for 2DC, 1-s average.

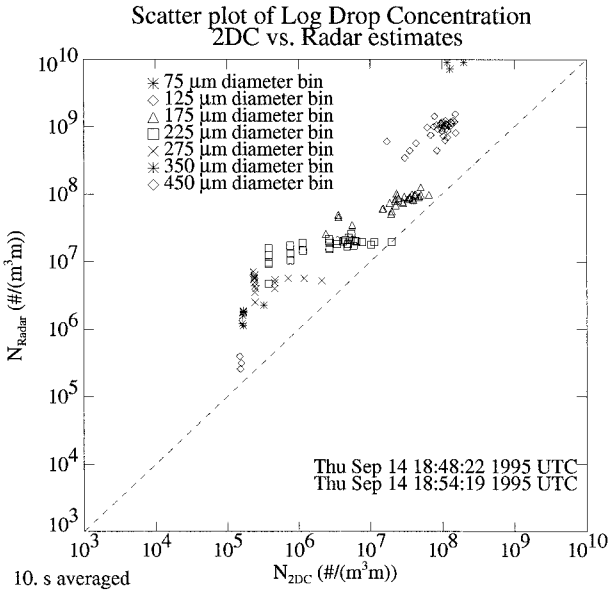

FIG. 11. Scatterplot of concentrations measured by 2DC and corresponding radar estimates of $N(D)$ for diameter bins reported for 2DC, 10-s average.

The 1-s average plot (Fig. 10) displays clear signs of quantization noise in the measurements of concentration density for the 175-μm bin and larger diameter bins. This is clear in the vertical line patterns at which the probes stop reporting lower concentration densities while the radar continues to do so. The 10-s average plot (Fig. 11) shows some signs of quantization but at much lower concentrations, as expected. This plot makes it clear that the radar and 2DC probe results correspond usually within an order of magnitude for the drops in the 125- and 175-μm bins. The data in the larger diameter bins have not yet converged enough to comment about the correspondence between the two systems. The 30-s average plot adds the 225-μm bin to the list of those displaying correspondence to within 1–1.5 orders of magnitude between the two systems. Further averaging left too few points for the comparison to be meaningful, given that there were only 358 points reported at 1-s intervals.

Some of the remaining discrepancy between the 2DC and radar measurements of $N(D)$ for the 125-, 175-, and 225-μm bins is likely due to calibration offsets and spectrum spreading, as detailed in the previous sections regarding errors expected in the measurements. There is also the distinct possibility that the distance between the observations (60-m range) explains some of the differences in the measurements. The degree of agreement present in the scatterplots, however, indicates that the calibration constant used for the radar power measurement conversion to reflectivity was correct to the degree visible from the scale on the scatterplots.

b. Spectral analysis of along-track variation for 2DC and radar N(D) measurements

To quantify the degree of common variation along the flight track in the 2DC and radar measurements of $N(D)$, the spectrum of the 2DC observations of $N(D)$ was calculated and plotted against the spectrum for the corresponding radar estimates for each diameter bin. The sample rate for the data, 1 Hz, allowed for a max-

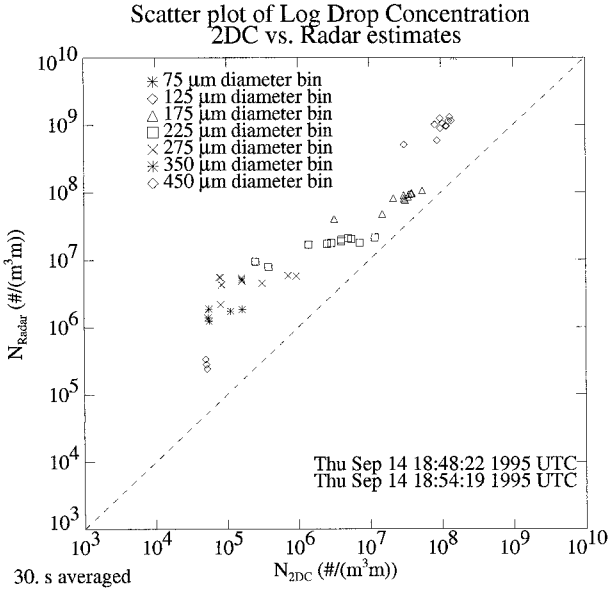

FIG. 12. Scatterplot of concentrations measured by 2DC and corresponding radar estimates of $N(D)$ for diameter bins reported for 2DC, 30-s average.

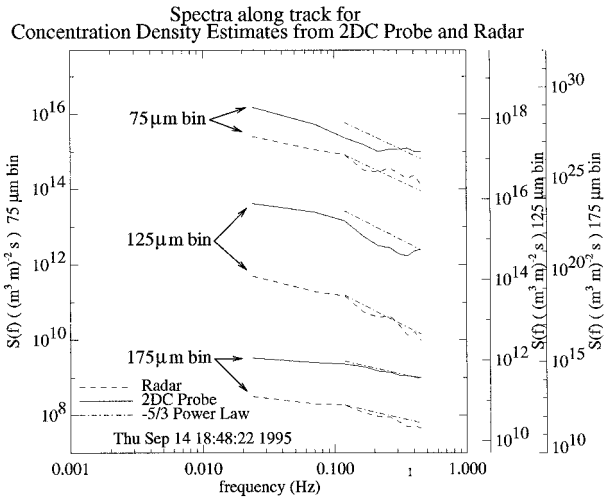

FIG. 13. Spectra along track of 2DC probe and radar concentrations for 75–775-μm bins. Note that a different ordinate scale is required for each diameter bin.

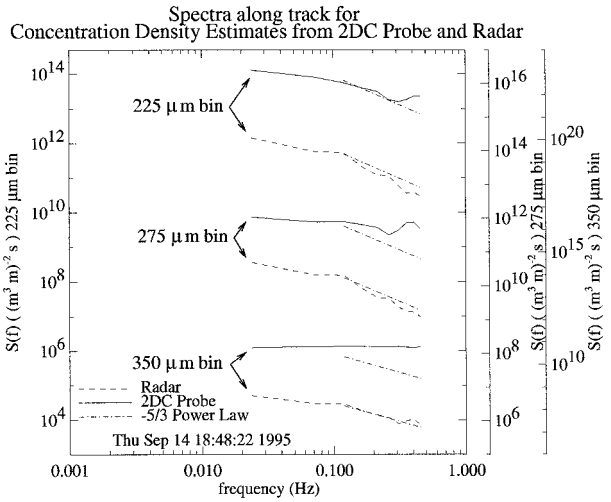

FIG. 14. Spectra along track of 2DC probe and radar concentrations for 225–350-μm bins. Note that a different ordinate scale is required for each diameter bin.

imum spectral frequency of 0.5 Hz. The power spectra were calculated from the available 358 samples along track using 39 point (N_p) Hanning windows, offset from one another by 19 points. The coefficients in the Hanning window were calculated as

$$w_q = 0.132\left\{1 + \cos\left[\frac{2\pi}{N_p}\left(q - \frac{N_p - 1}{2}\right)\right]\right\}, \quad (14)$$

which produces a window that scales the total variance in the spectrum by unity for a spectrum estimate of the given length. This window length was chosen to yield 18 (N_w) independent spectrum estimates to be averaged together. If one denotes the samples of concentration density along track by x_n, for either the probe or radar estimates at a given diameter bin, then the expression for the spectrum may be written

$$X_k = N_w^{-1} \sum_{l=0}^{N_w-1} \left| N_p^{-1} \sum_{q=0}^{N_p-1} w_q x_n e^{-j2\pi qk/N_p} \right|^2, \quad (15)$$

where X_k is the spectrum estimate at spectral frequency bin k, n is $19l + q$, and j is $\sqrt{-1}$. This meant that the standard deviation of the spectrum estimates was about 24% of the estimated value. This yielded a spacing between points in the spectra of 0.026 Hz with a maximum corresponding wavelength of 10 km and a minimum corresponding wavelength of 170 m.

The agreement between the 2DC spectra and radar spectra is quite pronounced (Figs. 13 and 14). Spectra were calculated for only those diameter bins for which there were significant data and a reasonable expectation that the series were related. For the most part, although the absolute value of the variance along track is not the same, the slopes of the variance with frequency are nearly the same, and both spectra in all cases except the 2DC data in the 275-and 350-μm bins (Fig. 14) follow an approximately $-5/3$ slope for the higher frequencies. Assuming that the higher spectral frequencies fall in the inertial subrange, statistical turbulence theory and unit analysis predict this kind of variation (Tatarskii 1971). Such variation has been observed in spectra of horizontal variation in reflectivity measurements in stratiform clouds (Henrion and Sauvageot 1977). This feature in both sets of spectra indicates that the conditions driving the variance in the measurements were naturally determined rather than instrument artifacts. The concentration estimates for the 275- and 350-μm bins were near the threshold of those detectable for both instruments; therefore, there were few drops of that size measured in the sampling interval available. This was the likely reason for the noiselike distribution of the variance in the 2DC spectrum for these bins. In the cases of the other bins for which spectra were plotted, the deviation in the spectrum from the $-5/3$ power law occurs at about 0.04 Hz, which would indicate that the factors contributing to variation in those concentration density measurements took place on a timescale of 25 s. Unfortunately, the available data do not conveniently support spectral analysis at a finer resolution with any greater confidence.

9. Conclusions

These results summarize the current state of research into using an airborne W-band radar to estimate $N(D)$ in liquid clouds. The techniques described here will be expanded to obtain radar estimates of $N(D)$ at ranges well beyond the 60 m considered here. The present analysis provides a basis for interpreting the radar estimates of $N(D)$ in comparison with microphysical probe measurements. The analysis of precision in the probe and radar measurements indicates that subsequent use of

probe data as compared with airborne W-band radar data should be undertaken with the understanding that a few to tens of seconds are required for the 2DC probe to converge to a reasonable value of $N(D)$, which may be compared with the radar data. Even longer averaging intervals will be required for the 1D probe.

One of the principal limitations to comparing the spectra measured with the radar and 2DC probe involves the minimum concentration of the 2DC probe relative to that of the radar. For larger drops, the radar has a clear advantage in making $N(D)$ measurements and moments thereof since its sample volume is larger and its sample rate higher. This advantage translates into the capability to characterize clouds and precipitation on much smaller horizontal scales (1-s average corresponds to 85 m along track in this case). The composition of the cloud observed must also be considered during such comparisons as the averaging performed will be influenced by the region over which the average is taken as much as by the interval in time.

This dataset has verified that, at least for stratiform clouds, aircraft motion removal was successful in correcting the measured velocities for purposes of $N(D)$ retrieval from the Doppler spectra. The same cannot yet be said of the air motion correction, as this case does not present a significant amount of air motion. Assuming that the air motion indicated by the aircraft INS does not change significantly between the immediate environment of the King Air and the resolution volume, there is no reason to expect the air motion removal to present a problem since that factor is indistinguishable from aircraft motion for purposes of Doppler velocity measurement. The scatterplots of 2DC and radar $N(D)$ values over long enough averaging intervals revealed that the radar calibration constant used to scale power to reflectivity was correct to the degree required to form estimates of $N(D)$ comparable to the probe values. The effects of turbulence, movement of the radar resolution volume during the measurement, and resolution volume separation between the probes and radar measurements remain as factors preventing the comparison between the radar and probe data to be closer. If a more thorough comparison is desired, the radar sampling should be closer to the probe sample volume and the spectra should be more finely resolved in velocity to allow a reasonable treatment of the effects of turbulence on the Doppler spectrum measurement. In addition, the removal of turbulence driven spectral spread will require estimation of the width of the turbulence spectrum.

The analysis of horizontal variation in both the 2DC and radar $N(D)$ values reveals that effects of the inertial subrange are visible in both the 2DC and radar spectra at the same scale lengths. This spectral analysis could stand improvement in terms of the resolution available in the frequency domain. This would require a dataset sampled over a longer period of time.

Verification of the match between the two different techniques supports the use of the radar estimate of $N(D)$ at ranges farther away than the closest range gate and for averaging intervals smaller than those required for the 2DC probe. Challenges remaining before such estimates may be reliably produced include the problem of estimating the attenuation between an observed region and the aircraft, and determining a reasonable estimate of the updraft velocity at distant points. Research oriented toward the further understanding of the relation between probe and radar measurements of liquid clouds and precipitation and use of more remote radar data in such cases should provide greater facility in interpreting the radar data in terms of the process of precipitation initiation.

Acknowledgments. The measurements discussed in this paper would not have been possible without the support of the following University of Wyoming staff: E. Gasaway, G. Gordon, P. Wechsler, K. Endsley, D. Lukens, and L. Irving. The analysis of the spectral variation of the measurements benefited greatly from discussions with Dr. Stephen Frasier of the University of Massachusetts Microwave Remote Sensing Laboratory. This work was made possible by NSF Grants ATM-9320672 to the University of Massachusetts and ATM-9319907 to the University of Wyoming, administered by Dr. Ron Taylor, Program Director, Physical Meteorology Program, Atmospheric Sciences Division.

REFERENCES

Atlas, D., R. Srivastava, and R. Sekhon, 1973: Doppler radar characteristics of precipitation at vertical incidence. *Rev. Geophys. Space Phys.,* **11,** 1–35.

Baumgardner, D., 1983: An analysis and comparison of five water droplet measuring instruments. *J. Appl. Meteor.,* **22,** 891–910.

——, 1989: Airborne measurements for cloud microphysics. *Res. Aviat. Facility Bull.,* **24,** 1–22.

Cerni, T., 1983: Determination of the size and concentration of cloud drops with an FSSP. *J. Climate Appl. Meteor.* **22,** 1346–1355.

Doviak, R., and D. Zrnić, 1993: *Doppler Radar and Weather Observations.* Academic Press, 562 pp.

Gossard, E. E., 1988: Measuring drop-size distributions in clouds with a clear-air-sensing doppler radar. *J. Atmos. Oceanic Technol.,* **5,** 640–649.

——, 1994: Measurement of cloud droplet size spectra by Doppler radar. *J. Atmos. Oceanic Technol.,* **11,** 712–726.

Henrion, X., and H. Sauvageot, 1977: Spectral analysis of stratiform cloud radar observations. *Geophys. Res. Lett.,* **4** (9), 360–362.

Heymsfeld, A., and J. Parrish, 1978: A computational technique for increasing the effective sampling volume of the PMS two-dimensional particle size spectrometer. *J. Appl. Meteor.,* **17,** 1566–1572.

Jenkins, G. M., and D. G. Watts, 1968: *Spectral Analysis and Its Applications.* Holden-Day, 525 pp.

Lhermitte, R. M., 1988: Observations of rain at vertical incidence with a 94-GHz Doppler radar: An insight on Mie scattering. *Geophys. Res. Lett.,* **15,** 1125–1128.

Meteorology Research, Inc., 1969: Universal Indicated Turbulence System, Model 1120. Meteorology Research, Inc., Altadena, CA.

Mie, G., 1908: Betirage zur Optik Truber Medien, Speziell Kolloidaler Metalasungen. *Ann. Phys.*, **25,** 377 pp.

Oppenheim, A. V., and R. W. Schafer, 1989: *Discrete-Time Signal Processing.* Prentice Hall, 879 pp.

Pazmany, A. L., R. E. McIntosh, R. Kelly, and G. Vali, 1994: An airborne 95-GHz dual-polarized radar for cloud studies. *IEEE Trans. Geosci. Remote Sens.*, **32** (4), 731–739.

Rogers, R. R., D. Baumgardner, S. A. Ethier, D. A. Carter, and W. L. Ecklund, 1993: Comparison of raindrop size distributions measured by radar wind profiler and by airplane. *J. Appl. Meteor.*, **32,** 694–699.

Tatarskii, V. I., 1971: *The Effects of the Turbulent Atmosphere on Wave Propagation.* Israel Program for Scientific Translation.

Ulaby, F., R. Moore, and A. Fung, 1982a: *Microwave Remote Sensing: Active and Passive.* Vol. 1. Artech House, 456 pp.

——, ——, and ——, 1982b: *Microwave Remote Sensing: Active and Passive.* Vol. 2. Artech House, 608 pp.

Zrnić, D. S., 1975: Simulation of weatherlike Doppler spectra and signals. *J. Appl. Meteor.*, **14,** 619–620.